Mathematical modeling of Fabry–Perot resonators: II. Uniformly converging multimode equivalent-circuit models

G. Hugh Song

Department of Physics and Photon Science, Gwangju Institute of Science and Technology, Gwangju 500-712, South Korea (hughsong@gist.ac.kr)

Received September 17, 2013; accepted December 12, 2013;
posted December 18, 2013 (Doc. ID 197742); published January 30, 2014

Based on complex-variable analysis of a Fabry–Perot resonator as a multimode nonsymmetric two-port waveguide device, two versions of equivalent-circuit configurations are presented: Starting from a renewed study on single-mode two-pole circuits, we develop two respective multimode equivalent circuits of an almost identical configuration: one for the reflection coefficient and the other for the pass-through transmission coefficient. In the mathematics language of complex-variable analysis, the two models successfully "approximate" the two scattering coefficients through two "uniformly converging" partial-fraction series expansions. © 2014 Optical Society of America

OCIS codes: (050.2230) Fabry-Perot; (070.5753) Resonators; (250.5300) Photonic integrated circuits.
http://dx.doi.org/10.1364/JOSAA.31.000411

1. INTRODUCTION

Almost all resonator-based waveguide devices in the frequency range from microwave to optical frequencies are basically designed based on the Fabry–Perot resonator (FPR) structure [1] or on its four-port variation [2]. To name a few waveguide resonators with two-holed diaphragms [3], standard bulk-optic FPRs, planar-optic ring resonators [4,5], photonic-crystal resonators [6], Bragg resonators [7], etc., belong to the broader class of FPRs in metal-tubic, microwave-monolithic, bulk-optic, and integrated-optic implementations throughout the radio to optical frequency ranges.

A good equivalent-circuit model for such a linear time-invariant electromagnetic device is always an efficient aid in understanding key features of the physical device under consideration. Exemplary use of such equivalent circuits for waveguide devices in microwave and optical science and engineering can be found, for example, recently in Ref. [7] as well as historically in Ref. [8] during the early years of microwave engineering.

Some elementary equivalent circuits for FPRs were employed in the analysis for a pair of holed diaphragms in microwaves [9,10], a mirror cavity in laser optics [11], and quarter-wave-shifted distributed-Bragg reflectors in integrated optics [12]. In ultrafast optics, use of such an equivalent-circuit model turned out to be especially effective in understanding the working principle of mode-locked lasers [13].

So far in literature, equivalent-circuit single-mode [13] and multimode [3] FPR models are analyzed mostly from phenomenological viewpoints. A certain multimode model, as the one in Ref. [3], may only be called an "input-equivalent multimode circuit," because the "output circuit" for pass-through is not realized explicitly. Losing too much rigor, such models do not even pass the basic impedance/admittance equivalence test.

Often, we find ourselves wishing to have accurate equivalent circuit models for FPRs of any kind to simply plug into some popular computerized circuit analysis programs, e.g., SPICE [14]. At this point, those existing single-fraction models cannot be used at all in any mid-frequencies between two adjacent resonance points in a FPR, while the mid-frequency response is also important for an error-free analysis of the pass-through port in the channel-drop filter [2,6]. Here, a uniformly converging model would do the job perfectly.

In this respect, we find that two ideal multimode electric-circuit models realizing the uniformly converging complex rational functions in an exact manner for a given FPR are desired:

1. one for the "reflection-equivalent model" for the reflection coefficient using only lumped circuit-elements and
2. the other for the "pass-through-equivalent model" that simulates the pass-through coefficient over the entire range of a free-spectral range.

A prerequisite complex-variable analysis for the spectral data is essential and the relevant work has been documented by the present author in Ref. [15]. Some key results from the latter work are presented below along with an introduction of important definitions and useful formulas for the work of the present part.

A. Proposition of Definitions and Needed Formulas for Modeling Fabry–Perot Resonators

Inside a cavity of a FPR, filled with a homogeneous medium of length d between two mirrors A and B, let $\beta(\omega)$ be the complex propagation constant for the lightwave at optical frequency ω. Without loss of generality, we suppose that any phase change inside the mirrors is absent, as was imposed in Eq. (8) in Ref. [15]. Then the jth resonance frequency ω_j is determined by

$$d \cdot \mathrm{Re}\,\beta(\omega_j) \equiv j\pi, \qquad j = 0, 1, 2, \ldots. \tag{1}$$

The fraction-reciprocated reflection coefficient for the wave incident through mirror A is given from Eq. (24) in Ref. [15] as

$$\frac{-1}{\vec{\mathcal{R}}(\omega)} = \frac{1}{r_\mathrm{A}} + \frac{h_\mathrm{A}^2/r_\mathrm{A} - r_\mathrm{A}}{\mathrm{e}^{-\mathrm{i}2\beta(\omega)d} r_\mathrm{A}/r_\mathrm{B} - h_\mathrm{A}^2} \tag{2}$$

in terms of positive parameters r_A and r_B of the two respective mirrors A and B, where

$$h_\mathrm{A} \equiv \sqrt{r_\mathrm{A}^2 + t_\mathrm{A}^2} \tag{3}$$

for mirror A, when t_A and t_B are positive parameters for the two pass-through coefficients for the respective mirrors. Here, the pass-through coefficient $\mathcal{T}(\omega)$ is related to $\vec{\mathcal{R}}(\omega)$ by a fundamental inter-relationship

$$\mathcal{T}(\omega) = -\frac{r_\mathrm{A} + \vec{\mathcal{R}}(\omega)}{r_\mathrm{B}} \frac{t_\mathrm{B}}{t_\mathrm{A}} \mathrm{e}^{-\mathrm{i}\beta(\omega)d}. \tag{4}$$

Henceforth in this paper, we presume that the FPR medium is dispersion-free for every resonance frequency for simplicity. Then,

$$\omega_j \equiv j\omega_1 = 2\pi j/\tau_\circlearrowleft, \qquad j = 0, 1, 2, \ldots \tag{5}$$

for round-trip time $\tau_\circlearrowleft \equiv 2d[\mathrm{Re}\, d\beta/d\omega]$ turning constant, whereas those reciprocated decay time constants

$$\gamma_\mathrm{A} \equiv -\ln r_\mathrm{A}/\tau_\circlearrowleft, \qquad \gamma_\mathrm{B} \equiv -\ln r_\mathrm{B}/\tau_\circlearrowleft, \tag{6}$$

$$\gamma^\mathrm{in} \equiv 2d\,\mathrm{Im}\,\beta(\omega)/\tau_\circlearrowleft \tag{7}$$

become mode-independent.

From our study in Ref. [15], for a FPR with two mirrors and the inner medium made of such a dispersion-less, reciprocal media, application of the logarithmic differentiation to Eq. (2) has yielded a partial-fraction series

$$\frac{-1}{\vec{\mathcal{R}}(\omega)} \equiv \eta_\mathrm{A} + \left[\frac{1}{r_\mathrm{A}} - \frac{r_\mathrm{A}}{h_\mathrm{A}^2}\right] \sum_{j=-\infty}^{\infty} \frac{\omega_1/2}{\mathrm{i}j\omega_1 + \vec{\gamma}^\circ - \mathrm{i}\omega}, \tag{8}$$

displaying the zeros of the complex-valued function explicitly, where

$$\eta_\mathrm{A} \equiv \frac{1}{2}\left[\frac{1}{r_\mathrm{A}} + \frac{r_\mathrm{A}}{h_\mathrm{A}^2}\right] \tag{9}$$

is the properly determined leading constant term worked out at Eq. (27) in Ref. [15]. Here,

$$\vec{\gamma}^\circ \equiv \gamma^\mathrm{in} - \gamma_\mathrm{A} + \gamma_\mathrm{B} - \tau_\circlearrowleft^{-1} \ln h_\mathrm{A}^2 \tag{10}$$

is nonzero in general from Eqs. (6) and (7) and is common for all resonance modes in such a FPR.

In the following presentation, we use Laplace-transform variable s for $-\mathrm{i}\omega$ rather than $k \equiv \mathrm{Re}\,\beta(\omega)$ in Ref. [15], giving an explicit expression for frequency dependence. We then introduce a finite series

$$\vec{\Sigma}^{(N)}(s) = [1/r_\mathrm{A} - r_\mathrm{A}/h_\mathrm{A}^2]\tau_\circlearrowleft^{-1} \times \left\{\frac{1}{\vec{\gamma}^\circ + s} + \sum_{j=1}^{N} \frac{2s + 2\vec{\gamma}^\circ}{[s + \vec{\gamma}^\circ]^2 + j^2\omega_1^2}\right\} \tag{11}$$

to pick up the summation term from Eq. (8) as

$$-1/\vec{\mathcal{R}}(\omega) = \eta_\mathrm{A} + \vec{\Sigma}^{(\infty)}(-\mathrm{i}\omega). \tag{12}$$

2. TWO-POLE SINGLE-MODE LUMPED-ELEMENT EQUIVALENT CIRCUITS

Only for the present section, we presume that the mirrors are lossless, so that the hypotenuses in Eq. (3)

$$h_\mathrm{A} = h_\mathrm{B} \to 1. \tag{13}$$

Actually, a lossy mirror plate may be treated as another lossy FPR, viz., a Fabry–Perot étalon, with two symmetric lossless reflecting surfaces. Therefore, in the fundamental level, the above condition is not so limiting.

Then, the two scattering coefficients in Eqs. (4) and (2) are expressed simply and conveniently as

$$\mathcal{T}(\omega) \to -\frac{\sqrt{\sinh[\gamma_\mathrm{A}\tau_\circlearrowleft]\sinh[\gamma_\mathrm{B}\tau_\circlearrowleft]}}{\sinh\{[\gamma^\mathrm{x} - \mathrm{i}\omega]\tau_\circlearrowleft/2\}}, \tag{14}$$

$$\begin{aligned}\vec{\mathcal{R}}(\omega) &\to -\frac{\sinh\{[\vec{\gamma}^\circ - \mathrm{i}\omega]\tau_\circlearrowleft/2\}}{\sinh\{[\gamma^\mathrm{x} - \mathrm{i}\omega]\tau_\circlearrowleft/2\}} \\ &= -\frac{\vec{\gamma}^\circ}{\gamma^\mathrm{x}} \prod_{j=-\infty}^{\infty} \frac{1 - \mathrm{i}\omega/[\vec{\gamma}^\circ + \mathrm{i}j\omega_1]}{1 - \mathrm{i}\omega/[\gamma^\mathrm{x} + \mathrm{i}j\omega_1]},\end{aligned} \tag{15}$$

respectively, for $\vec{\gamma}^\circ \to \gamma^\mathrm{in} + \tau_\circlearrowleft^{-1} \ln[r_\mathrm{A}/r_\mathrm{B}]$ from Eq. (10) with $h_\mathrm{A} \to 1$, whereas

$$\gamma^\mathrm{x} \equiv \gamma^\mathrm{in} + \gamma_\mathrm{A} + \gamma_\mathrm{B} \tag{16}$$

regardless of Eq. (13). The numerator in the right-hand side of Eq. (14) is to be implemented by

$$1/r_\mathrm{A} - r_\mathrm{A}/h_\mathrm{A}^2 \to 1/r_\mathrm{A} - r_\mathrm{A} \equiv 2\,\sinh[\gamma_\mathrm{A}\tau_\circlearrowleft] \tag{17}$$

as $h_\mathrm{A} \to 1$ according to Eq. (6).

Around a single selected resonance frequency ω_x of a highly reflective FPR, $\sinh[\gamma_\mathrm{A}\tau_\circlearrowleft] \to \gamma_\mathrm{A}\tau_\circlearrowleft$ in Eq. (17), the reflection coefficient for an incident wave from side A becomes

$$\vec{\Gamma}(s) \to \frac{2\gamma_\mathrm{A}}{s + \gamma^\mathrm{x} + \mathrm{i}\omega_\mathrm{x}} - 1 \tag{18}$$

approximately after retaining a single fraction. Evidently, this is equivalent to Collin [10] 2nd ed., Eq. (7.82) and to Haus [13] Eq. (7.37). They both presented a simple equivalent *LGC*-circuit approximating the above expression. All subsequent papers [2,6,16] of Haus and his co-workers accepted this proposal in their works.

Actually, the single-fraction formula in Eq. (18) is not physically realizable with any circuit elements, because a scattering data from any physical device, regardless of a real FPR or an equivalent circuit, must be symmetric with respect to the real

axis in the complex-s plane. Therefore, the proper single-mode expression must carry a pair of symmetric poles at $-\gamma^{\mathrm{x}} \pm \mathrm{i}\omega_{\mathrm{x}}$ for both scattering coefficients for the simplest possible circuit in Fig. 1.

A. Single-Mode Equivalent Admittance Circuit

First for Fig. 1, the *circuit* pass-through coefficient for voltage signals for the device inside the dashed-rectangular box is found as

$$\vec{\Upsilon}_V(s) = \frac{2Y_{\mathrm{A}}}{[Y_{\mathrm{A}} + Y_{\mathrm{B}} + G] + sC + 1/[R_{\mathrm{x}} + sL_{\mathrm{x}}]}. \tag{19}$$

We take

$$\overleftrightarrow{G} \equiv G + Y_{\mathrm{B}} + Y_{\mathrm{A}} \tag{20}$$

in the denominator, so that

$$\vec{\Upsilon}_V(s) = \frac{2Y_{\mathrm{A}}}{C} \cdot \frac{R_{\mathrm{x}}/L_{\mathrm{x}} + s}{[s - s_{\mathrm{x}}][s - s_{\mathrm{x}}^*]} \tag{21}$$

in terms of two poles, one at

$$s_{\mathrm{x}} = -\frac{1}{2}\left[\frac{\overleftrightarrow{G}}{C} + \frac{R_{\mathrm{x}}}{L_{\mathrm{x}}}\right] + \mathrm{i}\sqrt{\frac{1}{CL_{\mathrm{x}}} - \frac{1}{4}\left[\frac{\overleftrightarrow{G}}{C} - \frac{R_{\mathrm{x}}}{L_{\mathrm{x}}}\right]^2} \tag{22}$$

and its complex-conjugate s_{x}^*.

The corresponding reflection coefficient is found as

$$\vec{\Gamma}_V(s) \equiv \vec{\Upsilon}_V(s) - 1 = -\frac{s - \vec{s}_\circ}{s - s_{\mathrm{x}}} \cdot \frac{s - \vec{s}_\circ^*}{s - s_{\mathrm{x}}^*} \tag{23}$$

in terms of s_{x} above and

$$\vec{s}_\circ \equiv -\frac{1}{2}\left[\frac{\vec{G}}{C} + \frac{R_{\mathrm{x}}}{L_{\mathrm{x}}}\right] + \mathrm{i}\sqrt{\frac{1}{CL_{\mathrm{x}}} - \frac{1}{4}\left[\frac{R_{\mathrm{x}}}{L_{\mathrm{x}}} - \frac{\vec{G}}{C}\right]^2}, \tag{24}$$

$$\vec{G} \equiv G + Y_{\mathrm{B}} - Y_{\mathrm{A}} = \overleftrightarrow{G} - 2Y_{\mathrm{A}}. \tag{25}$$

The ultimate pass-through coefficient including the effect of the two impedance transformers is found by

$$\Upsilon_P(s) = \vec{\Upsilon}_V(s)\sqrt{Y_{\mathrm{B}}/Y_{\mathrm{A}}}, \tag{26}$$

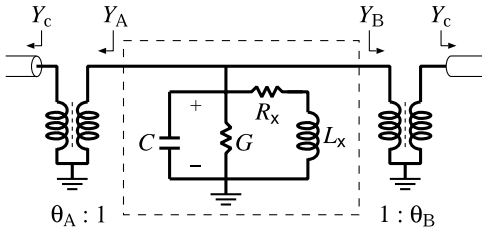

Fig. 1. Simple lumped-element equivalent circuit approximately representing a Fabry–Perot resonator (FPR) near one resonance frequency $\omega_{\mathrm{x}} \equiv \sqrt{1/L_{\mathrm{x}}C}$ among infinitely many such resonance frequencies. To match with the external wave admittance Y_{c}, two ideal admittance transformers with winding ratios θ_{A} and θ_{B} are attached.

distinguished from $\vec{\Upsilon}_V(s)$ at Eq. (21) based on the voltage signal. The modification makes the coefficient based on square-root-power amplitudes between the input and the output.

Based on some obvious connections to the parameters of a FPR, let us set

$$L_{\mathrm{x}}C \Rightarrow 1/\omega_{\mathrm{x}}^2, \tag{27}$$

$$\left\{\begin{matrix} Y_{\mathrm{A}}/C \\ Y_{\mathrm{B}}/C \end{matrix}\right\} \Rightarrow \frac{2}{\tau_{\circlearrowleft}} \left\{\begin{matrix} \sinh[\gamma_{\mathrm{A}}\tau_{\circlearrowleft}] \\ \sinh[\gamma_{\mathrm{B}}\tau_{\circlearrowleft}] \end{matrix}\right\} \simeq \left\{\begin{matrix} 2\gamma_{\mathrm{A}} \\ 2\gamma_{\mathrm{B}} \end{matrix}\right\}. \tag{28}$$

Next, we have two basic lossy circuit elements in the box at Fig. 1: resistance R_{x} in series to an inductance and conductance G in parallel to a capacitance. They together represent attenuation of the wave amplitude in the internal medium of the FPR, showing up as $R_{\mathrm{x}}/2L_{\mathrm{x}}$ and $G/2C$ in Eqs. (22) and (24). Hence, we set

$$R_{\mathrm{x}}/2L_{\mathrm{x}} + G/2C \Rightarrow \gamma^{\mathrm{in}} \tag{29}$$

from Eq. (7) as a reasonable condition, with which the scattering amplitudes of the spectral response near the resonance must fit with those of the corresponding true spectral response based on Eqs. (14) and (15).

B. Poles Set at the Resonance Frequency

It appears that we still have a freedom in choosing $R_{\mathrm{x}}/L_{\mathrm{x}}$. One can choose it so that either $\mathrm{Im}\, s_{\mathrm{x}}$ or $\mathrm{Im}\, \vec{s}_\circ$ may be set exactly at $\omega_{\mathrm{x}} \equiv 1/\sqrt{L_{\mathrm{x}}C}$, although, in a highly effective FPR with highly reflective mirrors, the difference becomes negligible. For the first circuit model however, we now choose

$$\mathrm{Im}\, s_{\mathrm{x}} = \omega_{\mathrm{x}}, \tag{30}$$

which will let the peak of resonance pass-through show up exactly at ω_{x} at Eq. (24). Indeed, the latter choice gives a simpler analysis than the other choice.

Let us thus choose

$$R_{\mathrm{x}}/L_{\mathrm{x}} = \overleftrightarrow{G}/C \Rightarrow \gamma^{\mathrm{x}} \equiv \gamma^{\mathrm{in}} + \gamma_{\mathrm{B}} + \gamma_{\mathrm{A}}, \tag{31}$$

$$G/C \Rightarrow \gamma^{\mathrm{in}} - \gamma_{\mathrm{B}} - \gamma_{\mathrm{A}}, \tag{32}$$

satisfying Eqs. (16) and (29). As a model, having a negative parameter in either G yielding $\mathrm{Re}\, \vec{s}_\circ > 0$ does not matter. Overall passiveness is determined by $\mathrm{Re}\, s_{\mathrm{x}} < 0$. Hence, the imaginary part of the pole set at

$$s_{\mathrm{x}} \equiv -\gamma^{\mathrm{x}} + \mathrm{i}\omega_{\mathrm{x}} \Leftarrow -\overleftrightarrow{G}/C + \mathrm{i}/\sqrt{CL_{\mathrm{x}}} \tag{33}$$

at Eq. (22) coincides with $\omega_{\mathrm{x}} \equiv 1/\sqrt{L_{\mathrm{x}}C}$ exactly, whereas

$$\vec{s}_\circ = -\vec{\gamma}^\circ + \mathrm{i}\sqrt{\omega_{\mathrm{x}}^2 - 4\gamma_{\mathrm{A}}^2} \tag{34}$$

follows from Eq. (24) with $\vec{G}(s)$ at Eq. (25).

With the choice of Eqs. (31) and (32), the partial-fraction expansion of Eq. (21) gives

$$\vec{\Upsilon}_V(s) \Rightarrow 2\frac{\sinh[\gamma_A \tau_{\circlearrowleft}]}{\tau_{\circlearrowleft}} \cdot \frac{2s + 2\gamma^x}{[s+\gamma^x]^2 + \omega_x^2} \simeq \frac{4\gamma_A}{s_x - s_x^*}\left[\frac{s_x}{s - s_x} - \frac{s_x^*}{s - s_x^*}\right], \tag{35}$$

$$\vec{\Gamma}_V(s) = \vec{\Upsilon}_V(s) - 1. \tag{36}$$

Therefore, under $\gamma^x \ll 2\omega_1$, which is absolutely reasonable in a functioning resonator, we have

$$\vec{\Gamma}_V(-i\omega_x) \equiv \vec{\Upsilon}_V(-i\omega_x) - 1 \simeq \frac{2\gamma_A}{\gamma^x} - 1 = -\frac{\vec{\gamma}^\circ}{\gamma^x}, \tag{37}$$

which is consistent with $\vec{\mathcal{R}}(\omega_x) = -\vec{\gamma}^\circ/\gamma^x$ at Eq. (15).

Finally, the ideal admittance/impedance transformers transform the admittance and impedance. For instance,

$$Y_A \equiv Y_c \theta_A^2, \qquad Y_B \equiv Y_c \theta_B^2, \tag{38}$$

where θ_A:1 and 1:θ_B are the winding ratios indicated for mirrors A and B, respectively, in Fig. 1(b). Neither the overall power pass-through transmittivity nor the reflectivity is affected by presence of these transformers.

In terms of square-root power amplitudes, we multiply $\sqrt{\gamma_B/\gamma_A}$ in the right-hand side according to $\Upsilon_P(s) \equiv \vec{\Upsilon}_V(s)\sqrt{Y_B/Y_A}$ at Eq. (26):

$$\Upsilon_P(s) \Rightarrow 2\sqrt{\gamma_A \gamma_B}\left[\frac{1 + i\gamma^x/\omega_x}{s + \gamma^x - i\omega_x} + \frac{1 - i\gamma^x/\omega_x}{s + \gamma^x + i\omega_x}\right]. \tag{39}$$

C. Zeros Set at the Resonance Frequency in the Dual Circuit

One can make up a circuit dual to Fig. 1 almost trivially, as shown in Fig. 2. This could have been made with $\Upsilon_V(s)$ and $\vec{\Gamma}_V(s)$ being replaced trivially by $\vec{\Upsilon}_I(s)$ and $\vec{\Gamma}_I(s)$ after standard substitution of R_x/L_x, G/C by G_1/C_1, $[R' + R''_\Gamma]/L$ in Fig. 2.

We now ask whether we can obtain an alternative two-pole model with the focus on the equivalent reflection coefficient rather than the equivalent pass-through coefficient. It is the second choice,

$$\mathrm{Im}\,\vec{s}_\circ = \omega_1, \tag{40}$$

which would result in a dip of the reflectivity appearing exactly at ω_1 at Eq. (24). We thus propose the dual circuit with a new set of parameters to represent the reflection coefficient more closely than the pass-through coefficient as follows:

First, we partition R into two parts: R' and R''_Γ in expressing the circuit pass-through coefficient as

$$\vec{\Upsilon}_I(s) = \frac{2Z_A}{\underbrace{Z_A + Z_B + R''_\Gamma} + R' + sL + \frac{1}{G_1 + sC_1}} \tag{41}$$

by considering R' as a part of an elementary resonator circuit with the four parameters satisfying $R'/L = G_1/C_1$. This resonator circuit may pass the signal at resonance without minimal reflection when the so-called *reflectionless matching condition*

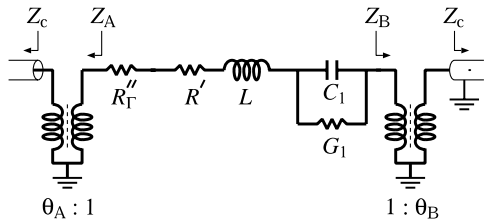

Fig. 2. Circuit configuration that is dual to that of Fig. 1. To simulate the two paired zeros of $\vec{\Gamma}_I(s)$, circuit parameters are not to be chosen exactly dual to those of Fig. 1.

$$Z_A + Z_B + R''_\Gamma = 2Z_A \tag{42}$$

is satisfied at resonance. This condition lets $\vec{\Gamma}_I(s) \equiv \vec{\Upsilon}_I(s) - 1$ be expressed simply by its fraction-reciprocal

$$\frac{-1}{\vec{\Gamma}_I(s)} = 1 + \frac{2Z_A}{R' + sL + 1/[G_1 + sC_1]}. \tag{43}$$

A few basic circuit parameters are set as usual:

$$LC_1 \Rightarrow 1/\omega_1^2, \tag{44}$$

$$\left\{\begin{matrix} Z_A/L \\ Z_B/L \end{matrix}\right\} \Rightarrow \frac{2}{\tau_{\circlearrowleft}}\left\{\begin{matrix} \sinh[\gamma_A \tau_{\circlearrowleft}] \\ \sinh[\gamma_B \tau_{\circlearrowleft}] \end{matrix}\right\} \simeq \left\{\begin{matrix} 2\gamma_A \\ 2\gamma_B \end{matrix}\right\}, \tag{45}$$

all in parallel to Eqs. (27) and (28). The basic pair of zeros of $\vec{\Gamma}_I(s)$ for the single-mode resonator is set by

$$R'/L = G_1/C_1 \Rightarrow \vec{\gamma}^\circ \equiv \gamma^{in} - \gamma_A + \gamma_B \tag{46}$$

in contrast to $\overleftrightarrow{G}/C = R_1/L_1$ at Eq. (31). Then,

$$\frac{-1}{\vec{\Gamma}_I(s)} \simeq 1 + 2\gamma_A\left[\frac{1}{s + \vec{\gamma}^\circ + i\omega_1} + \frac{1}{s + \vec{\gamma}^\circ - i\omega_1}\right], \tag{47}$$

contrasting the prior choice of $\vec{s}_\circ$ and $\vec{s}_\circ^*$ for the zeros of $\vec{\Gamma}_V(s)$ at Eq. (34). Even more directly than Eq. (37), under $\gamma^x \ll 2\omega_1$ of a good resonator, one can confirm that the model Eq. (47) gives

$$\frac{-1}{\vec{\Gamma}_I(-i\omega_1)} \simeq 1 + \frac{2\gamma_A}{\vec{\gamma}^\circ} = 1 + \frac{\gamma^x - \vec{\gamma}^\circ}{\vec{\gamma}^\circ} = \frac{\gamma^x}{\vec{\gamma}^\circ}, \tag{48}$$

which is approximately consistent with Eq. (15) and with Eq. (37). These points are of importance when we develop any multimode equivalent circuits for a FPR shortly.

Finally, the same ideal transformers transform the termination impedance:

$$Z_A \equiv Z_c/\theta_A^2, \qquad Z_B \equiv Z_c/\theta_B^2 \tag{49}$$

in a fashion that is fraction-reciprocal to Eq. (38). From now on, we will consider, not the original characteristic admittance and impedance but the mirror admittance and impedance.

So far, the presented two-pole *RLGC* resonator-circuit models in Figs. 1 and 2 may be considered as trivial improvements over the prior approximate ones in textbooks utilizing either an *RLC* configuration in Ref. [17] or an *LGC*

configuration in literatures, e.g., in Ref. [13] Fig. 7.2 and in Ref. [10] 2nd ed., Fig. 7.28.

3. MULTIMODE REFLECTION-EQUIVALENT CIRCUIT

In such single-pole or single-mode approximation, it did not make much sense to make any effort to obtain an approximation better than what we say something decent. Through the present study on the multimode equivalent-circuit models for general FPRs, some fundamental issues in guided-wave optics are to be addressed and be answered:

1. whether it is truly possible to devise a lumped-circuit multimode-equivalent model for a FPR, which represents both the reflection and transmission coefficient,
2. whether the *LGC* model is sufficient or whether the *RLGC* model is necessary in principle,
3. how the delay-line circuit element represents the physical size of the resonator,
4. how and whether we can accommodate the offset constant of the partial-fraction expansion in Ref. [15] in multimode equivalent circuits for a FPR, etc.
5. whether we can make a full generalization for any type of cavity resonators, beside a regular-looking FPR, with somewhat nonuniform resonance frequencies.

Any actual FPR is inherently a multimode device. Such a multimode FPR model requires a keen eye into some of the fundamental principles of electromagnetics. Each single-mode circuit of Fig. 2 impedes the passage of the signal unless the frequency of the signal matches the resonance frequency. Therefore, for the number of resonance modes being simulated, we may augment as many such series-*RLGC* resonator circuits in parallel as would "admit" a signal around any of those resonance frequencies, as illustrated in Fig. 3, in which we have proposed an auxiliary conductance on top of the resonator block.

A. Reflection Coefficient for an Enlarged Resonator-Circuit Array

Let us suppose that we have a finite number of N resonators in the array. Then, the total driving-point impedance of the circuit with a finite number of *RLGC*-resonators in the array must be $Z_{\rm dp}(s) \equiv R''_\Gamma + 1/\vec{Y}^{(N)}_\Gamma(s) + Z_{\rm B}$, where

$$\vec{Y}^{(N)}_\Gamma(s) \equiv \bar{G}_\Gamma + 1/Z_0(s) + \cdots + 1/Z_N(s) \tag{50}$$

is the impedance for an array of N resonators indicated in the diagram in Fig. 2 with

$$\frac{1}{Z_0(s)} \equiv \frac{1}{2R' + s2L} = \frac{1/2L}{R'/L + s}, \tag{51}$$

$$\frac{1}{Z_j(s)} = \frac{1/L}{R'/L + s + [1/LC_j]/[G_j/C_j + s]} \tag{52}$$

for $j = 1, 2, \ldots, N$.

Incidentally, a formula similar to Eq. (50), without the crucial first term $\bar{G}_\Gamma$, appeared in Ref. [18] for the simulation of a *short-circuited* lossless transmission line, which could be interpreted as a resonator by itself. The formula did not correctly recognize the role of $\bar{G}_\Gamma$ for the resulting transmission-line resonator.

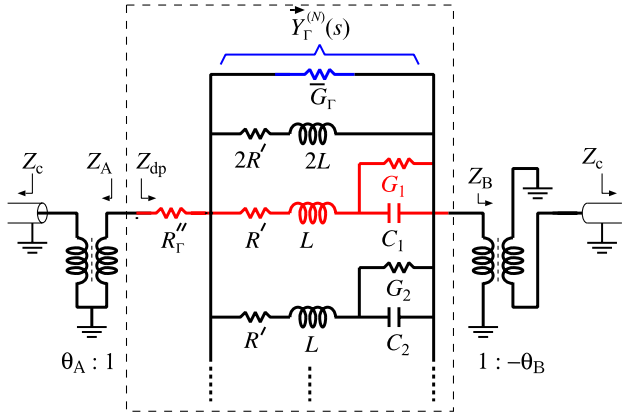

Fig. 3. Multimode reflection-equivalent lumped-circuit model for a FPR supporting a large number of modes by implementing as many unit resonators, in the shape of Fig. 2.

With the circuit array of Fig. 3 enlarged from that of Fig. 2, the circuit pass-through coefficient is found as

$$\vec{\Upsilon}^{(N)}_I(s) = \frac{2Z_{\rm A}}{\underbrace{Z_{\rm A} + Z_{\rm B} + R''_\Gamma} + 1/\vec{Y}^{(N)}_\Gamma(s)}, \tag{53}$$

replacing $\vec{\Upsilon}_I(s)$ in Eq. (41). In search for an equivalent circuit representing Eq. (8), we let the latter three ω-independent terms in the numerator of

$$\vec{\Gamma}^{(N)}_I(s) \equiv 1 - \vec{\Upsilon}^{(N)}_I(s) \tag{54}$$

disappear by letting the expression in Eq. (53) be a continued fraction by choosing

$$R''_\Gamma = Z_{\rm A} - Z_{\rm B} \tag{55}$$

as in Eq. (42) for compensation for the difference in the two terminations for a general nonsymmetric FPR.

Such an enforced symmetric impedance termination in turn lets the functional shape of $-1/\vec{\Gamma}^{(N)}_I(s)$ agree with that of Eq. (8):

$$-1/\vec{\Gamma}^{(N)}_I(s) = 1 + 2Z_{\rm A}\vec{Y}^{(N)}_\Gamma(s) \Rightarrow \eta_{\rm A} + \vec{\Sigma}^{(N)}(s) \tag{56}$$

with

$$2Z_{\rm A}\bar{G}_\Gamma \Rightarrow \eta_{\rm A} - 1, \tag{57}$$

$$2Z_{\rm A}\sum_{j=0}^{N}\frac{1}{Z_j(s)} \Rightarrow \vec{\Sigma}^{(N)}(s), \tag{58}$$

which is consistent with Eq. (11). The sum of the latter two expressions is to be projected at

$$2Z_{\rm A}\vec{Y}^{(N)}_\Gamma(s) \Rightarrow \vec{\Sigma}^{(N)}(s) + \eta_{\rm A} - 1 \tag{59}$$

of Eq. (11) by noticing that the functional shape of each term of $\vec{\Sigma}^{(\infty)}(s)$ in Eq. (11) is exactly identical to that of Eqs. (51) and (52). Hence, in a straightforward manner, the similarity suggests one should implement as many *RLGC*-resonator

circuits as possible to simulate the true reflection coefficient of the FPR.

That is, impedance Z_A and Z_B expressing out-coupling through the mirrors are determined by

$$\left\{\begin{matrix} Z_A/L \\ Z_B/L \end{matrix}\right\} \Rightarrow \frac{1}{\tau_{\circlearrowleft}} \left\{\begin{matrix} 1/r_A - r_A/h_A^2 \\ 1/r_B - r_B/h_B^2 \end{matrix}\right\} \tag{60}$$

slightly modified from Eq. (45) for nonunity h_A^2 in the multimode equivalent circuit. For Eqs. (51) and (52), the resonance frequencies of a FPR must give the capacitance values as

$$1/LC_j \Rightarrow \omega_j^2 \equiv j^2\omega_1^2 \tag{61}$$

extended from Eq. (44). Further, we need again

$$G_j/C_j = R'/L \Rightarrow \vec{\gamma}^{\circ} \equiv \gamma^{\text{in}} + \gamma_B - \gamma_A - \tau^{-1} \ln h_A^2 \tag{62}$$

also modified from Eq. (46) for nonunity h_A in all places in the circuit array, except two arms: the one with

$$2L\bar{G}_\Gamma \Rightarrow \frac{\tau_{\circlearrowleft}[\eta_A - 1]}{1/r_A - r_A/h_A^2} = \frac{\tau_{\circlearrowleft}}{2} \frac{1/r_A + r_A/h_A^2 - 2}{1/r_A - r_A/h_A^2} \tag{63}$$

from Eq. (57) combined with Eq. (60) and the one denoted by $2R'$ and $2L$ in Fig. 3. To match the ratio between the first fraction and the rest in Eq. (11), we should have $2R'$ and $2L$ in the first arm, eventually promoting L as one of the "base" parameters of the model.

Because the resulting circuit in Fig. 3 is an exact representation of Eq. (58), we may expect that we will get the predicted spectral responses as already analyzed in thick solid curve in Fig. 7 in Ref. [15] and in the thick dashed curve in Fig. 6 in [15]. Verification of our conclusion on the two reflection coefficients is made with $N = 6$ this time for the plot of Fig. 4(a). For this plot and all others that follow, we keep the parameter values of the FPR that we used for Fig. 3 in [15].

B. Pass-Through Coefficient with the Multimode Reflection-Equivalent Circuit

If we wish to maintain the same circuit of Fig. 3 to simulate the square-root-power-based pass-through coefficient of the same FPR as well as its reflection coefficient, we would just use the well-established standard relationship Eq. (54) with the necessary revision of Eq. (26) from the already proposed reflection-equivalent circuit:

$$\vec{\Upsilon}_P^{(N)}(s) \equiv [\vec{\Gamma}_I^{(N)}(s) + 1]\sqrt{Z_B/Z_A}. \tag{64}$$

The plot for $\vec{\Upsilon}_P^{(6)}(-i\omega)$ is made and compared with $\mathcal{T}(\omega)$ from the original FPR at Eq. (4) in Fig. 4(b). We find that the degree of agreement with $\mathcal{T}(\omega)$ represented by thin curves is sufficiently impressive *in the pass-bands* around successive resonance frequencies. However, appearance of the unavoidable π phase hops happening at those successive resonances has made a serious disagreement in the imaginary parts and ultimately in the power spectral data, shown in Fig. 4(c), at mid-frequencies between adjacent resonance points.

In order to remove the base disagreement in the plot for the phase of the pass-through coefficient in Eq. (64), one can

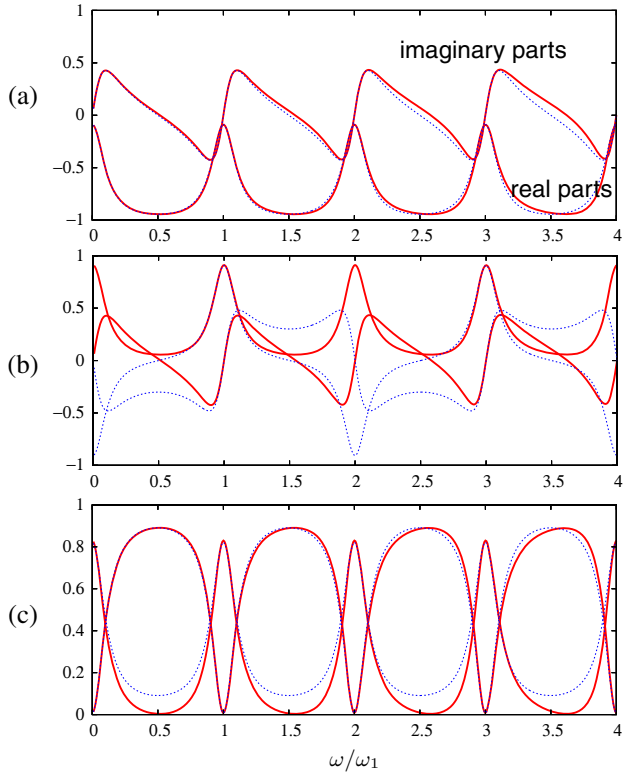

Fig. 4. Spectral responses of the reflection-equivalent circuit for a FPR in thick curves from the circuit model of Fig. 3 in comparison with the actual response in thin dotted curves. (a) Real and imaginary parts of the reflection coefficient $\vec{\Gamma}_I^{(6)}(-i\omega)$ of Eq. (56). (b) Those of the pass-through coefficient for the circuit-based interpretation $\vec{\Upsilon}_P^{(6)}(-i\omega)$ at Eq. (64). (c) Reflectivity $|\vec{\Gamma}_I^{(6)}(-i\omega)|^2$ and the pass-through transmittivity $|\vec{\Gamma}_I^{(6)}(-i\omega) + 1|^2 Z_B/Z_A$. For all plots in this study, we use $h_A = h_B = 1$, $r_A = r_B = 0.7304$, giving $\gamma_A/\omega_1 = \gamma_B/\omega_1 = 0.05$ and $\gamma^{\text{in}}/\omega_1 = 0.01$. In comparison, the two thin curves are made for the real and imaginary parts of $\mathcal{R}(\omega)$ in Eq. (15) for the corresponding FPR.

trivially add a *negative delay line* of length d in addition to the transformer illustrated in Fig. 3 with a negative winding ratio. The resulting plot for $-\vec{\Upsilon}_P^{(N)}(-i\omega)e^{-i\omega\tau_{\circlearrowleft}/2}$ is given in Fig. 5. Unfortunately, although the phase-hop is removed, overall agreement with $\mathcal{T}(\omega)$ is still not satisfactory.

Considering the implication from the plots of Figs. 5 and 4(b), we must conclude that the proposed reflection-equivalent circuit model of Fig. 3 (without any revision of the circuit configuration) comes up short at simulating the pass-through multimode transmission spectrum of a FPR especially at the mid-frequencies, unless the FPR has an extremely high Q-number.

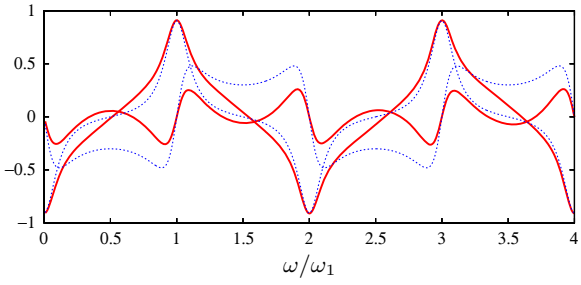

Fig. 5. Real and imaginary parts of $-[\vec{\Gamma}_I^{(6)}(-i\omega) + 1]\, e^{-i\omega\tau_{\circlearrowleft}/2}\sqrt{Z_B/Z_A}$. The thin curves represent $\mathcal{T}(\omega)$ from the original FPR.

C. Discussion on the Multimode Reflection-Equivalent Circuit

Note first that, beyond the purpose of numerical verification, from the projection of the circuit model in terms of partial fractions, there is no need for any delay or decay element before the array of resonators in the equivalent circuit, because the array itself represents the action of such delay and decay elements.

Note also that, as before with Eq. (46), the sign of $G_j/C_j = R'/L$ follows that of $\vec{\gamma}^{\circ}$ according to Eq. (62). This sign will turn out to be negative if $e^{\gamma^{\text{in}}\tau_{\circlearrowleft}} r_A/h_A^2 r_B < 1$. Although it may not look pretty, as a mathematical and computational *model*, negative values for those negative circuit parameters do not impose any limitation of an equivalent circuit.

Also, as mentioned in Eq. (49), to recover the original characteristic wave impedances Z_c of the external waveguides rather than Z_A and Z_B, we need to use two transformers in Fig. 3 with nonunity winding ratios for θ_A and θ_B following Eq. (49). Neither the negative winding ratio for the impedance-matching transformer nor the negative delay line of length $-d$ denoted near the end of the equivalent circuit in Fig. 3 affects the reflection coefficient being simulated.

The effect of the auxiliary conductance $\bar{G}_\Gamma$ is well demonstrated in Fig. 4(c). At resonance, power will be zero-impeded toward the side of "mirror B" through the resonator array rather than the side door $\bar{G}_\Gamma$. Hence, the power pass-through would hardly be affected at resonance. On the other hand, in mid-frequencies between adjacent resonance points, effective pass-through is even further reduced than $|\mathcal{T}(\omega)|^2$, because $\bar{G}_\Gamma$ is draining the incident wave power without transferring the power to the "B side." Such a draw of power is required for a faithful representation of the reflection coefficient, but not for a good representation of the pass-through coefficient, which is well demonstrated in Fig. 4(c).

In Ref. [15], we mentioned that the change of preceding constant at Eq. (2) from $1/r_A$ to $\eta_A \equiv [1/r_A + r_A/h_A^2]/2$, resulting in proper parameterization of $\bar{G}_\Gamma$, used to be called "renormalization" in the infinite-order perturbation. The structure of infinite feedback that is so evident in a multimode FPR is one such example that anyone can easily depict. Yet, we have seen that, *in single-mode representations* at Eq. (37) and at Eq. (48), if implemented, such an offset would only have caused trouble rather than any improvement in terms of accuracy.

As we worked with dual circuits in Figs. 1 and 2, one can compose a second circuit configuration dual to Fig. 3. That is, the dual circuit employs an array of individual admittance resonators all connected in series as depicted in Fig. 6.

4. MULTIMODE PASS-THROUGH-EQUIVALENT CIRCUIT

If we return to Fig. 4(b), we find that, beside the π-phase hop at successive pass-bands, the spectral match over the pass-bands is so impressive that we may ask whether we should bother with any improvement in the mid-frequencies. More often, however, FPRs are used as optical filters, in which the pass-through coefficient is more important than the reflection coefficient. Therefore, it is worth finding another ideal equivalent circuit for the true pass-through coefficient $\mathcal{T}(\omega)$ in Eq. (14):

Up to the task of finding a better revision, we investigate the exact relationship in Eq. (4) between the true scattering

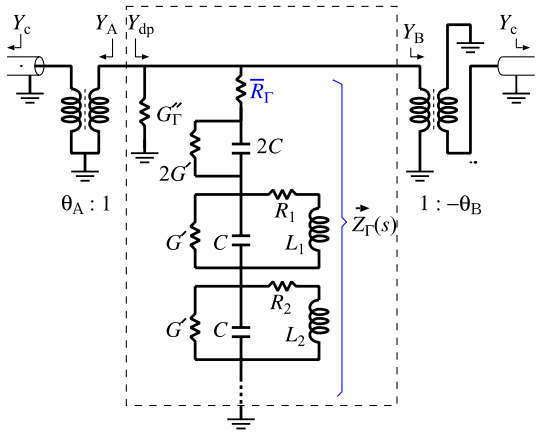

Fig. 6. Circuit dual to the one in Fig. 3. $R_j, L_j, G', C, G''_\Gamma, \bar{R}_\Gamma$ here replace $G_j, C_j R', L, R''_\Gamma, \bar{G}_\Gamma$, respectively, in Fig. 3.

coefficients of a FPR. Inserting $\vec{\mathcal{R}}(\omega) \Leftarrow \vec{\Gamma}_I^{(\infty)}(-i\omega)$ of Eq. (56) into it, we have

$$\mathcal{T}(\omega) \equiv -\frac{t_B e^{-i\beta(\omega)d}}{t_A r_B}\left[r_A + \frac{-1}{\eta_A + \vec{\Sigma}^{(\infty)}(-i\omega)}\right] \tag{65}$$

with $\vec{\Sigma}^{(N)}(s)$ from Eq. (11).

In order to make the above expression well-projected to the pass-through coefficient of a certain circuit to be determined, we rewrite Eq. (65) as

$$\mathcal{T}(\omega) = -e^{\gamma^{\text{in}}\tau_{\circlearrowleft}/2 - i\omega\tau_{\circlearrowleft}/2} t_B r_A / t_A r_B \times \left\{1 + \frac{-1}{1 - [1 - \eta_A r_A] + r_A \vec{\Sigma}^{(\infty)}(-i\omega)}\right\}, \tag{66}$$

where

$$1 - \eta_A r_A = 1/2 - r_A^2/2h_A^2 \equiv t_A^2/2h_A^2 \tag{67}$$

from Eq. (60) will be used shortly. Here, the shape of the last expression is guided by that of the pass-through coefficient across the resonator array as

$$\vec{\Upsilon}_I^{(N)}(s) \equiv \frac{2Z_A}{Z_A + Z_B + R''_\Upsilon + 1/\vec{Y}_\Upsilon^{(N)}(s)} = \frac{2Z_A}{Z_A + Z_B + R''_\Upsilon} \cdot \frac{\vec{Y}_\Upsilon^{(N)}(s)}{\vec{Y}_\Upsilon^{(N)}(s) + \frac{1}{Z_A + Z_B + R''_\Upsilon}} \tag{68}$$

in terms of

$$\vec{Y}_\Upsilon^{(N)}(s) \equiv \bar{G}_\Upsilon + 1/Z_0(s) + 1/Z_1(s) + \cdots \tag{69}$$

similar to Eq. (50) beside the leading term $\bar{G}_\Upsilon$ given in the pass-through-equivalent circuit of Fig. 7 replacing $\bar{G}_\Gamma$ in Fig. 3.

To compare the latter expression with Eq. (66), we rewrite the latter in terms of the square-root-power-based pass-through coefficient in a shape of

$$\Upsilon_P^{(N)}(s) = \frac{2\sqrt{Z_A Z_B}}{Z_A + Z_B + R''_\Upsilon} \times \left\{ 1 + \frac{-1}{1 + [Z_A + Z_B + R''_\Upsilon]\vec{Y}_\Upsilon^{(N)}(s)} \right\} \tag{70}$$

with $\vec{Y}_\Upsilon^{(N)}(s)$ from Eq. (69). In determining the circuit parameters of the new pass-through equivalent circuit that is in many respects similar to the prior one, we must decide what to keep and what to change among the recipe parameters for the reflection-equivalent circuit. Some of the basic parameters such as $Z_A/2L$, $Z_B/2L$, LC_j, and $G_j/C_j = R'/L$ in Eqs. (60)–(62) are all carried intact.

With this much carry-over, comparison between Eqs. (66) and (70) still keeping Eq. (58) in

$$[Z_A + Z_B + R''_\Upsilon][\bar{G}_\Upsilon + 1/Z_0(s) + 1/Z_1(s) + \cdots] \Rightarrow r_A \vec{\Sigma}^{(\infty)}(s) - t_A^2/2h_A^2 \tag{71}$$

lets us choose

$$[Z_A + Z_B + R''_\Upsilon]/2Z_A \Rightarrow r_A, \tag{72}$$

rather than unity at Eq. (42), i.e.,

$$\frac{R''_\Upsilon}{Z_A} = 2r_A - 1 - \frac{1/r_B - r_B/h_B^2}{1/r_A - r_A/h_A^2} \simeq 2r_A - 1 - \frac{\gamma_B}{\gamma_A}, \tag{73}$$

with Z_A as given in Eq. (60) and $Z_B/Z_A \tilde{\Rightarrow} \gamma_B/\gamma_A$ at Eq. (17). This choice then breaks the condition of $Z_A = Z_B + R''_\Upsilon$ in Eq. (55) for impedance matching for minimal reflection at resonance. Evidently, in the pass-through-equivalent circuit, unlike the case of the reflection-equivalent circuit in Eq. (55), such property is not maintained.

Next, we need to make up for the difference in the overall factor by a power attenuator/amplifier with the gain $\vec{A}$ in Fig. 7, so that the prefactors agree between Eq. (66) and Eq. (70),

$$\frac{2\sqrt{Z_A Z_B}}{Z_A + Z_B + R''_\Upsilon}\vec{A} \Rightarrow \frac{t_B r_A}{t_A r_B} e^{\gamma^{in}\tau_\circlearrowleft/2}, \tag{74}$$

i.e.,

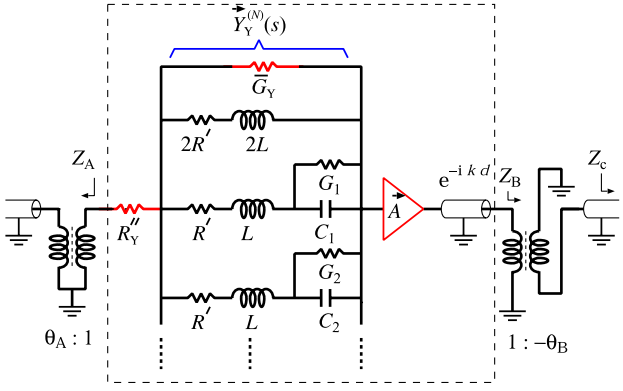

Fig. 7. Pass-through-equivalent circuit for a true FPR supporting infinitely many modes.

$$\vec{A} \Rightarrow r_A\sqrt{r_A/r_B} \cdot e^{\gamma^{in}\tau_\circlearrowleft/2} h_B/h_A, \tag{75}$$

and install it.

Finally, the auxiliary conductance $\bar{G}_\Upsilon$ is determined by utilizing Eq. (72) and Eq. (60) onto

$$[Z_A + Z_B + R''_\Upsilon]\bar{G}_\Upsilon = 2\frac{Z_A + Z_B + R''_\Upsilon}{2Z_A}\frac{Z_A}{2L} 2L\bar{G}_\Upsilon, \tag{76}$$

which must agree with $-t_A^2/2h_A^2$ at Eqs. (66) and (67). With respect to the "base" parameter $2L$, $\bar{G}_\Upsilon$ is determined by

$$2L\bar{G}_\Upsilon \Rightarrow -\tau_\circlearrowleft/2. \tag{77}$$

The negative conductance in the equivalent circuit would lower down the reflectivity at mid-frequencies, as indicated in Fig. 8(c). Evidently, if the loss coefficient of the internal medium of a FPR is large, $\vec{A}$ can become greater than unity.

With everything implemented properly, we should be obtaining the pass-through transmission coefficient as plotted in Fig. 8(a). The plot for $\vec{\Gamma}^{(6)}(-i\omega)$ and the power spectra are given in Figs. 8(b) and 8(c), respectively, for this pass-through-equivalent circuit. To match the proper complex ratio between the reflection coefficient and the pass-through coefficient, the negative delay line, representing the phase advance of $-kd$, after the equivalent circuit is necessary. The

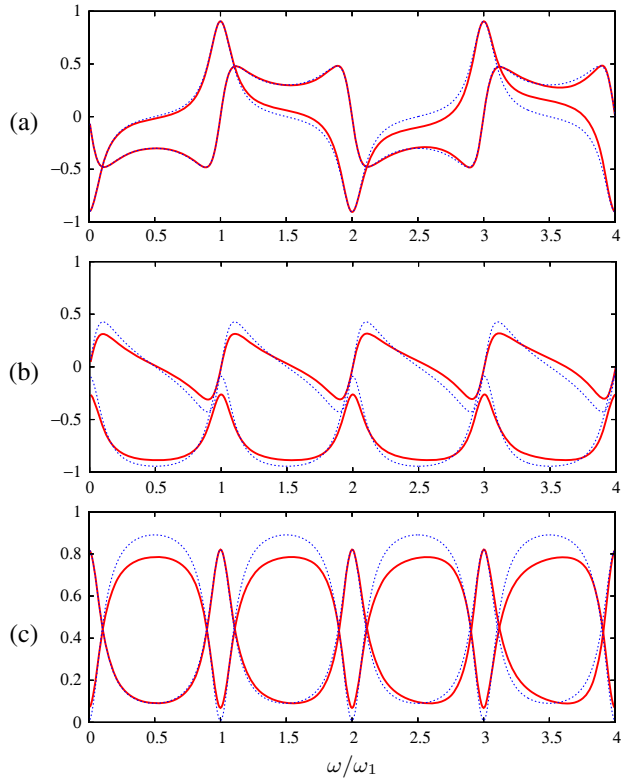

Fig. 8. Spectral responses of the pass-through-equivalent circuit for a FPR in thick curves from the circuit model with six *RLGC* resonators and an amplified/attenuated phase-delay line in comparison with the actual response in thin dotted curves. (a) Real and imaginary parts of the pass-through coefficient $\Upsilon_P^{(6)}(-i\omega)$ from Eq. (66), (b) the resulting reflection coefficient $\vec{\Gamma}_I^{(6)}(-i\omega)$, and (c) their power spectra in thick curves from the pass-through-equivalent circuit model.

best physical interpretation on this ambiguity would be that the lumped circuit is actually simulating a "*FPR squeezed into a single point in space.*"

Another minor point that deserves a mention is the fact that the zeroth resonance frequency of $\omega_0 \equiv 1/\sqrt{LC_0} = 0$ is implemented by the "infinite capacitance," i.e., *absent* capacitor, at the top of the array of Fig. 3. It can be explained by the fact that any static electric field may exist between two parallel mirrors as an exhibition of the zeroth resonance mode.

5. REMARKS ON THE MULTIMODE EQUIVALENT CIRCUITS

We have presented two versions of multimode equivalent circuits simulating a single FPR: a reflection-equivalent version and a pass-through-equivalent version that employs active and delay elements. Interestingly, in terms of required circuit elements, the two circuits show almost the same configuration. Only a few circuit parameters are different. Depending on the application, we are to choose one between the two choices.

Therefore, we provide answers to the questions that were given when we started Section 3:

1. Unlike the case of a single-mode equivalent circuit, for multimode equivalence, one circuit configuration cannot serve both scattering coefficients.
2. Considering Eqs. (32) and (46), a circuit with all four *RLGC* elements is far superior to either an *RLC* or an *LGC* circuit.
3. A negative-delay line is required for exact agreement of the formulas for the pass-through coefficient. However, it is basically a dummy device.
4. Implementation of an offset conductance element, $\bar{G}_\Gamma$ or $\bar{G}_\Upsilon$, is crucial for *multimode-equivalent* circuits, whereas any such augmentation would produce an inferior result in a single-mode equivalent circuit.
5. The basic configuration of a FPR can be generalized to a more complicated one with detailed information on, say, $\vec{\gamma}_j^{\circ}$ and $\gamma_j^{\times}$, denoted by mode index j, both depending on each of $\{\omega_0, \omega_1, \omega_2, \cdots\}$ that may not be equidistant in general. The offset $-1/2$ at Eq. (C8) in Ref. [15] is known to be valid for the case with equidistant zeros of the reflection coefficient along a straight line in the complex-k plane as Fig. 2 in Ref. [15]. Therefore, one must be careful in setting the right offset number for such a general case of a resonator.

Quite naturally, one may wish to use a common circuit model for both the reflection and pass-through coefficients, although the circuit becomes only nonuniformly approximating to either coefficient. Obviously, one would eliminate the auxiliary conductance altogether, i.e., $\bar{G}_\Gamma = 0$ in Fig. 3, because such a value is more or less the median between true $\bar{G}_\Gamma$ and $\bar{G}_\Upsilon$.

Figure 9 shows the resulting plots, in which agreement in the mid-frequencies is not satisfactory in all three plots. However, the disagreement would become negligible for FPRs with high Q number, e.g., $\gamma_A\omega_1 = \gamma_B\omega_1 = \gamma^{\text{in}}\omega_1 = 0.01$, as demonstrated in Fig. 10, although the circuit *cannot* be said to be *uniformly* approximating to the actual FPR response.

Yet, such a single representative but "nonuniformly" approximate model evidently allows cascading circuit models

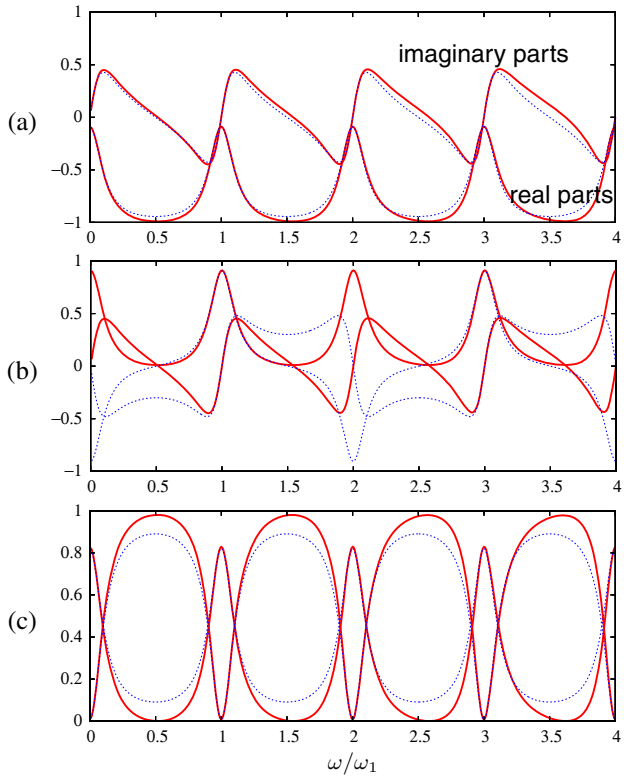

Fig. 9. Real and imaginary parts of (a) $\vec{\Gamma}^{(6)}(-i\omega)$, (b) $-[\vec{\Gamma}^{(6)}(-i\omega)+1]\sqrt{Z_B/Z_A}$, and (c) the reflectivity $|\vec{\Gamma}^{(6)}(-i\omega)|^2$ and the pass-through transmittivity $|\vec{\Gamma}^{(6)}(-i\omega)+1|^2 Z_B/Z_A$ all with $\vec{\Gamma}^{(6)}(-i\omega)$ in solid thick curves from the circuit of Fig. 3 without the auxiliary conductance, viz., $\bar{G}_\Gamma = 0$. The thin dotted curves represent the original FPR.

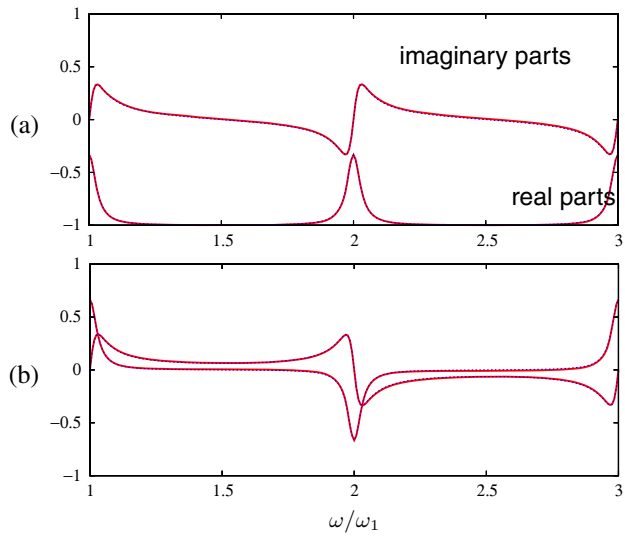

Fig. 10. Spectral response of a common equivalent circuit with $\bar{G}_\Gamma = 0$ in Fig. 3, for simulating both the reflection coefficient and the pass-through coefficient in thick solid curves over a range $2 < \omega/\omega_1 < 3$ for a FPR with more reflective mirrors with $r_A = r_B = 0.9391$ than those in the FPR with $r_A = r_B = 0.7304$ in all other plots in the paper. The curves almost coincide with the thin dotted curved from the analytic responses, which are actually hidden behind the thick curves: (a) $\vec{\Gamma}^{(6)}(-i\omega)$. (b) $\vec{\Upsilon}^{(6)}(-i\omega)e^{-i\omega\tau_\circlearrowleft/2}$.

in a network with no extra effort. Practically, FPRs are designed to be of even higher Q than the one demonstrated in Fig. 10.

6. CONCLUSION

Based on complex-variable analysis on the formula for scattering coefficients of a FPR in our prior study, we have successfully developed two multimode-equivalent circuit models, with which one can emulate the given FPR with uniform convergence: One model is made for emulating the reflection-coefficient formula and the other one is made separately for emulating the pass-through-coefficient formula. With all the circuit parameters determined by the two proposed recipes with as many resonator modules as possible, the spectral response of the presented circuit models would become exact, viz., are *uniformly converging* to the true spectral responses of the given FPR.

Hence, depending on applications, one may use the newly found appropriate multimode models in systemic general-purpose computerized circuit-based simulation tasks. Practically, one may appreciate a common approximate model for a given FPR, which has analyzed in addition to the exact models. Indeed, we have shown that a single representative FPR model would be sufficient for many well-designed high-Q resonators for both the passband and the reflection band that appears in mid-range frequencies between every two adjacent resonance frequencies.

The present study in two parts, which includes the study in Ref. [15], has sprung up from a pedantic curiosity on expressing some fundamental properties of a basic optical device in a rigorous mathematical manner, which may be appreciated in education. Therefore, beyond applications, the developed models serve as ideal aids in illustrating the basic functions of any passive electromagnetic resonators that include FPRs.

ACKNOWLEDGMENTS

I would like to thank Prof. Sang-Yung Shin of the Korea Advanced Institute of Science and Technology for his kind and special comments on the manuscript. Discussions with colleague Prof. Jae-Hyung Jang of GIST are greatly appreciated. This work was supported in part by the Top-Brand Research Program in the Gwangju Institute of Science and Technology (GIST).

REFERENCES

1. C. Fabry and A. Pérot, "Théorie et applications d'une nouvelle méthodes de spectroscopie interférentielle," Annal. Chim. Phys. **16**, 115–144 (1899).
2. H. A. Haus and Y. Lai, "Narrow-band optical channel-dropping filter," J. Lightwave Technol. **10**, 57–62 (1992).
3. R. E. Collin, *Foundations for Microwave Engineering*, 2nd ed. (IEEE, 1992), Fig. 7.30.
4. E. A. J. Marcatilli, "Bends in optical dielectric waveguides," Bell Syst. Tech. J. **48**, 2103–2132 (1969).
5. I. Ohtomo and S. Shimada, "A channel channel-dropping filter using ring resonators for the millimeter wave communication system," Trans. Inst. Electron. Commun. Eng. Jpn. **52-B**, 265–272 (1969).
6. K. Hwang and G. H. Song, "Design of a high-Q channel add-drop multiplexer based on the two-dimensional photonic-crystal membrane structure," Opt. Express **13**, 1948–1957 (2005).
7. A. Melloni, M. Floridi, F. Morichetti, and M. Martinelli, "Equivalent circuit of Bragg gratings and its applications to Fabry–Pérot cavities," J. Opt. Soc. Am. A **20**, 273–281 (2003).
8. C. G. Montgomery, R. H. Dicke, and E. M. Purcell, eds., *Principles of Microwave Circuits* (McGraw-Hill, 1948).
9. W. Culshaw, "Resonators for millimeter and submillimeter wavelengths," IRE Trans. Microwave Theory Technol. **MTT-9**, 135–144 (1961).
10. R. E. Collin, *Foundations for Microwave Engineering*, 1st ed. (McGraw-Hill, 1966).
11. A. E. Siegman, *Lasers* (University Science, 1986), pp. 934–939.
12. H. A. Haus and Y. Lai, "Theory of cascaded quarter wave shifted distributed feedback resonators," IEEE J. Quantum Electron. **28**, 205–213 (1992).
13. H. A. Haus, *Waves and Fields in Optoelectronics* (Prentice-Hall, 1984), Fig. 9.9.
14. T. Quarles, D. Pederson, R. Newton, A. Sangiovanni-Vincentelli, and C. Wayne, *SPICE3 Version 3f3 User's Manual* (University of California, 1993), The SPICE Page http://bwrcs.eecs.berkeley.edu/Classes/IcBook/SPICE/.
15. G. H. Song, "Mathematical modeling of Fabry–Perot resonators: I. Complex-variable analysis by uniformly convergent partial-fraction expansion," J. Opt. Soc. Am. A **31**, 404–410 (2014)
16. C. Manolatou, M. J. Khan, S. Fan, P. R. Villeneuve, H. A. Haus, and J. D. Joannopoulos, "Coupling of modes analysis of resonant channel add-drop filters," IEEE J. Quantum Electron. **35**, 1322–1331 (1999), Eq. (14).
17. A. Karp, H. J. Shaw, and D. K. Winslow, "Circuit properties of microwave dielectric resonators," IEEE Trans. Microwave Theor. Technol. **MTT-16**, 818–828 (1968).
18. R. Beringer, "Resonant cavities as microwave circuit elements," in *Principles of Microwave Circuits*, C. G. Montgomery, R. H. Dicke, and E. M. Purcell, eds. (McGraw-Hill, 1948), Chap. 7, Sect. 7.3.